Physics Letters B 732 (2014) 285–297

Contents lists available at ScienceDirect

Physics Letters B

www.elsevier.com/locate/physletb

Quintom phase-space: Beyond the exponential potential

Genly Leon [a], Yoelsy Leyva [a,b,*], J. Socorro [b]

[a] Instituto de Física, Pontificia Universidad Católica de Valparaíso, Casilla 4950, Valparaíso, Chile
[b] Departamento de Física, DCI, Universidad de Guanajuato-Campus León, C.P. 37150, León, Guanajuato, Mexico

ARTICLE INFO

Article history:
Received 26 February 2013
Received in revised form 21 March 2014
Accepted 28 March 2014
Available online 1 April 2014
Editor: S. Dodelson

ABSTRACT

We investigate the phase-space structure of the quintom dark energy paradigm in the framework of spatially flat and homogeneous universe. We have also included radiation and dark matter, both matter components are described as perfect fluids. Considering arbitrary decoupled potentials, we find certain general conditions under which the phantom-dominated solution is a late time attractor, generalizing previous results found for the case of an exponential potential. Center Manifold Theory is employed to obtain sufficient conditions for the instability of de Sitter solution either with phantom or quintessence potential dominance.

1. Introduction

Recent cosmological observations point to a strong evidence for a spatially flat and accelerated expanding universe [1–3]. Despite the great agreement of observations with the concordance model [4],[1] it is a fact that quintom model, whose Equation of State (EoS) can cross the cosmological constant barrier $w = -1$, is not excluded by observations [5–13]. A popular way to realize a viable quintom model and, at the same time, avoid the restrictions imposed by the *No-Go Theorem* [14–18] is the introduction of extra degrees of freedom.[2] Following this recipe, the simplest quintom paradigm requires a canonical quintessence scalar field σ and simultaneously a phantom scalar field ϕ where the effective potential can be of arbitrary form, while the two components can be either coupled [20] or decoupled [6,21].

The properties of the quintom models have been studied from different points of view. Among them, the phase space studies, using the dynamical systems tools, are very useful since they permit to bypass the complexities and non-linearities of the cosmological models, allowing to get insight into the asymptotic and intermediate behavior of solutions [22,23]. In quintom models this program has been carried out in [18,20,21,24–28]. In [21], the decoupled case between the canonical and phantom fields with an exponential potential was studied showing that the phantom-dominated scaling solution is the unique late-time attractor. In [20], the authors considered a potential with an interaction between the fields and show that, in the absence of interactions, the solution dominated by the phantom field should be the attractor of the system and the interaction does not affect its attractor behavior. However, in [24] it was shown that this result is correct only in the case in which the existence of the phantom phase excludes the existence of scaling attractors. Some of these previous results were extended in [25] to arbitrary potentials. Finally in [28], the authors showed that all quintom models with nearly flat potentials converge to a single expression for EoS of dark energy; in addition, the necessary conditions for the determination of the direction of the $w = -1$ crossing were found.

Another interesting feature concerning quintom models is that some potentials can be constructed using the Bohm-like approach [29–31], known as amplitude-real-phase formalism [32]. This scheme was used in [33] to derive the corresponding quintom potentials that emerge from quantum cosmology and provide a physical context for those potentials.[3] Among all the potentials found, only $V(\sigma,\phi) = V_0 \sinh^2(\alpha\sigma) + V_1 \cosh^2(\beta\phi)$ and $V(\sigma,\phi) = V_0 \exp[\pm(\alpha\sigma + \beta\phi)]$ satisfy the quantum constraint of this approach [33].

The objective of this paper is to investigate the dynamics of a general quintom dark energy model with the aim of finding viable scenarios that provide a crossing of the cosmological constant barrier (phantom divide) at low redshift and at the same time, extend the previous results in the literature [18,21,24–26]. We will

* Corresponding author.
E-mail addresses: genly.leon@ucv.cl (G. Leon), yoelsy.leyva@ucv.cl (Y. Leyva), socorro@fisica.ugto.mx (J. Socorro).

[1] The Cosmological Constant Model.

[2] The only way to realize the crossing without any ghosts and gradient instabilities in standard gravity and with one single scalar degree of freedom was obtained in [19].

[3] In the sense that, some potentials can be constructed [29,30,33].

http://dx.doi.org/10.1016/j.physletb.2014.03.053

investigate a wide variety of potentials, for which there is no interaction between the fields, by using the dynamical systems tools. In order to be able to analyze self-interaction potentials beyond the exponential one, we rely on the method introduced in the context of quintessence models [34] and that have been generalized to several cosmological contexts like: Randall–Sundrum II and DGP branes [35–38], Scalar Field Dark Matter models [39], tachyon and phantom fields [40–42] and loop quantum gravity [43].

The plan of the paper is as follows. In Section 2 we introduce the quintom model for arbitrary potentials and in Section 3 we build the corresponding autonomous system. The results of the study of the corresponding critical points, their stability properties and the physical discussion are shown in Section 4. Section 5 is devoted to conclusions.

Finally, we include two appendices, Appendix A and Appendix B, with the center manifold calculation of the solutions dominated by either the phantom or quintessence potential, respectively.

2. The model

The starting action of our model, containing the canonical field σ and the phantom field ϕ, is [6,20,21]:

$$S=\int d^4x\sqrt{-g}\Big(\frac{1}{2}R-\frac{1}{2}g^{\mu\nu}\partial_\mu\sigma\partial_\nu\sigma+V_\sigma(\sigma)+\frac{1}{2}g^{\mu\nu}\partial_\mu\phi\partial_\nu\phi+V_\phi(\phi)+\mathcal{L}_r+\mathcal{L}_m\Big), \tag{1}$$

where we used natural units ($8\pi G=1$) and $V_\sigma(\sigma)$ and $V_\phi(\phi)$ are respectively the self interaction potentials of the quintessence and phantom fields. The term $\mathcal{L}_r$ accounts for the radiation content of the universe, with energy density ρ_r and pressure P_r connected by the equation of state $\rho_r=P_r/3$, and $\mathcal{L}_m$ accounts for pressureless dark matter with energy density ρ_m and pressure $P_m=0$. From this action the Friedmann equations for a flat Friedmann–Lemaître–Robertson–Walker (FLRW) geometry reads [20,21]:

$$H^2=\frac{1}{3}\Big(\frac{\dot\sigma^2}{2}+V_\sigma(\sigma)-\frac{\dot\phi^2}{2}+V_\phi(\phi)+\rho_m+\rho_r\Big), \tag{2a}$$

$$\dot H=-\frac{1}{2}\Big(\dot\sigma^2-\dot\phi^2+\rho_m+\frac{4}{3}\rho_r\Big), \tag{2b}$$

where $H=\frac{\dot a}{a}$ is the Hubble parameter and the dot denotes derivative with respect the time. The conservation equations for the matter components leads to

$$\dot\rho_m=-3H\rho_m, \tag{3a}$$

$$\dot\rho_r=-4H\rho_r, \tag{3b}$$

while the evolution of the quintessence and phantom fields are:

$$\ddot\sigma+3H\dot\sigma+V'_\sigma(\sigma)=0 \tag{4a}$$

$$\ddot\phi+3H\dot\phi-V'_\phi(\phi)=0, \tag{4b}$$

where the prime $'$ denotes the derivative of a function with respect to its argument.

Additionally we can introduce the total energy density and pressure for the dark energy as:

$$\rho_{DE}=\rho_\sigma+\rho_\phi,\qquad p_{DE}=p_\sigma+p_\phi \tag{5}$$

where

$$\rho_\sigma=\frac{\dot\sigma^2}{2}+V_\sigma(\sigma),\qquad \rho_\phi=-\frac{\dot\phi^2}{2}+V_\phi(\phi) \tag{6}$$

$$p_\sigma=\frac{\dot\sigma^2}{2}-V_\sigma(\sigma),\qquad p_\phi=-\frac{\dot\phi^2}{2}-V_\phi(\phi) \tag{7}$$

and the equation of state parameter of the dark energy component is given by

$$w_{DE}=\frac{p_\sigma+p_\phi}{\rho_\sigma+\rho_\phi}=\frac{\dot\sigma^2-\dot\phi^2-2V_\sigma(\sigma)-2V_\phi(\phi)}{\dot\sigma^2-\dot\phi^2+2V_\sigma(\sigma)+2V_\phi(\phi)}. \tag{8}$$

Alternatively, we introduce the total (effective) equation of state parameter as:

$$w_{tot}=\frac{p_{tot}}{\rho_{tot}}=\frac{3\dot\sigma^2-3\dot\phi^2-6V_\sigma(\sigma)-6V_\phi(\phi)+2\rho_r}{3\dot\sigma^2-3\dot\phi^2+6V_\sigma(\sigma)+6V_\phi(\phi)+6\rho_r+6\rho_m}. \tag{9}$$

For convenience, we also introduce the dimensionless energy densities

$$\Omega_\sigma=\frac{\rho_\sigma}{3H^2}, \tag{10a}$$

$$\Omega_\phi=\frac{\rho_\phi}{3H^2}, \tag{10b}$$

$$\Omega_r=\frac{\rho_r}{3H^2}, \tag{10c}$$

$$\Omega_m=\frac{\rho_m}{3H^2}, \tag{10d}$$

which are related through[4]:

$$\Omega_\sigma+\Omega_\phi+\Omega_r+\Omega_m=1. \tag{11}$$

3. The autonomous system

In order to study the dynamical properties of the system (2a)–(4b), we introduce the following dimensionless phase space variables to build an autonomous dynamical system [44,45]:

$$x_\sigma=\frac{\dot\sigma}{\sqrt{6}H},\qquad x_\phi=\frac{\dot\phi}{\sqrt{6}H}, \tag{12a}$$

$$y_\sigma=\frac{\sqrt{V_\sigma(\sigma)}}{\sqrt{3}H},\qquad y_\phi=\frac{\sqrt{V_\phi(\phi)}}{\sqrt{3}H}, \tag{12b}$$

$$\lambda_\sigma=-\frac{V'_\sigma(\sigma)}{V_\sigma(\sigma)},\qquad \lambda_\phi=-\frac{V'_\phi(\phi)}{V_\phi(\phi)}, \tag{12c}$$

and the additional variables Ω_r and Ω_m defined by (10c) and (10d) respectively. Using the constraint (11) one is able to eliminate one degree of freedom, namely the variable y_ϕ. Notice that the phase space variables, λ_σ and λ_ϕ, are sensitive of the kind of self interaction potentials chosen for quintessence and phantom components, respectively and are introduced in order to be able to study arbitrary potentials. Applying the above dimensionless variables to the system (2a)–(4b), we obtain the following autonomous system:

$$\frac{dx_\sigma}{dN}=3x_\sigma^3+x_\sigma\Big(\frac{3\Omega_m}{2}-3x_\phi^2+2\Omega_r-3\Big)+\sqrt{\frac{3}{2}}\lambda_\sigma y_\sigma^2, \tag{13a}$$

$$\frac{dx_\phi}{dN}=-3x_\phi^3+x_\phi\Big(\frac{3\Omega_m}{2}+3x_\sigma^2+2\Omega_r-3\Big)+\sqrt{\frac{3}{2}}\lambda_\phi\big(x_\sigma^2-x_\phi^2+\Omega_m+\Omega_r+y_\sigma^2-1\big), \tag{13b}$$

$$\frac{dy_\sigma}{dN}=\frac{1}{2}y_\sigma\big(3\Omega_m+6x_\sigma^2-\sqrt{6}\lambda_\sigma x_\sigma-6x_\phi^2+4\Omega_r\big), \tag{13c}$$

[4] This relationship is obtained by substituting the above definitions (10) in the Friedmann equation (2a).

Table 1
Properties of the critical points for the autonomous system (13). The upper asterisk is used to denote values of λ_σ and λ_ϕ such that $\lambda_\sigma \in f^{-1}(0)$ and $\lambda_\phi \in g^{-1}(0)$, i.e., $f(\lambda_\sigma^*)=0$ and $g(\lambda_\phi^*)=0$, respectively. We use the definition $\frac{1}{\lambda^2}=\frac{1}{(\lambda_\sigma^*)^2}-\frac{1}{(\lambda_\phi^*)^2}$.

Label	x_σ	y_σ	x_ϕ	λ_σ	λ_ϕ	Ω_r	Ω_m	Existence	Stability
$P_1^\pm$	0	0	$\pm i$	λ_σ	λ_ϕ^*	0	0	Non-real	Unstable
$P_2^\pm$	± 1	0	0	λ_σ^*	λ_ϕ	0	0	$\lambda_\phi \in \mathbb{R}$	Unstable
$P_3^\pm$	$\pm\sqrt{1+x_\phi^2}$	0	x_ϕ	λ_σ^*	λ_ϕ^*	0	0	Always	Unstable
P_4	$\frac{\lambda_\sigma^*}{\sqrt{6}}$	$\sqrt{1-\frac{(\lambda_\sigma^*)^2}{6}}$	0	λ_σ^*	λ_ϕ	0	0	$(\lambda_\sigma^*)^2 \leqslant 6$	Saddle
P_5	0	0	0	λ_σ	0	0	0	$\lambda_\sigma \in \mathbb{R}$	Saddle
P_6	0	1	0	0	λ_ϕ	0	0	$\lambda_\phi \in \mathbb{R}$	Saddle
P_7	0	y_σ	0	0	0	0	0	$0 < y_\sigma < 1$	Stable for $f(0)>0$, $g(0)<0$, saddle otherwise
P_8	0	0	$-\frac{\lambda_\phi^*}{\sqrt{6}}$	λ_σ	λ_ϕ^*	0	0	$\lambda_\sigma \in \mathbb{R}$	Stable for $g'(\lambda_\phi^*)\lambda_\phi^*<0$, saddle otherwise
P_9	0	0	0	λ_σ	λ_ϕ	1	0	$\lambda_\sigma, \lambda_\phi \in \mathbb{R}$	Saddle
P_{10}	$\frac{2\sqrt{\frac{2}{3}}}{\lambda_\sigma^*}$	$\frac{2}{\sqrt{3}\sqrt{(\lambda_\sigma^*)^2}}$	0	λ_σ^*	λ_ϕ	$1-\frac{4}{(\lambda_\sigma^*)^2}$	0	$(\lambda_\sigma^*)^2 \geqslant 4$	Saddle
P_{11}	$\frac{2\sqrt{\frac{2}{3}}}{\lambda_\sigma^*}$	$\frac{2}{\sqrt{3}\sqrt{(\lambda_\sigma^*)^2}}$	$\frac{2\sqrt{\frac{2}{3}}}{\lambda_\phi^*}$	λ_σ^*	λ_ϕ^*	$1-\frac{4}{\lambda^2}$	0	$0 \leqslant \frac{4}{\lambda^2} \leqslant 1$	Saddle
P_{12}	0	0	0	λ_σ	λ_ϕ	0	1	$\lambda_\sigma, \lambda_\phi \in \mathbb{R}$	Saddle
P_{13}	$\frac{\sqrt{\frac{3}{2}}}{\lambda_\sigma^*}$	$\sqrt{\frac{3}{2(\lambda_\sigma^*)^2}}$	0	λ_σ^*	λ_ϕ	0	$1-\frac{3}{(\lambda_\sigma^*)^2}$	$(\lambda_\sigma^*)^2 \geqslant 3$	Saddle
P_{14}	$\frac{\sqrt{\frac{3}{2}}}{\lambda_\sigma^*}$	$\sqrt{\frac{3}{2(\lambda_\sigma^*)^2}}$	$\frac{\sqrt{\frac{3}{2}}}{\lambda_\phi^*}$	λ_σ^*	λ_ϕ^*	0	$1-\frac{3}{\lambda^2}$	$0 \leqslant \frac{3}{\lambda^2} \leqslant 1$	See discussion at the end of Section 4.1

$$\frac{d\Omega_r}{dN}=\Omega_r\big(3\Omega_m+6x_\sigma^2-6x_\phi^2+4(\Omega_r-1)\big), \tag{13d}$$

$$\frac{d\Omega_m}{dN}=\Omega_m\big(3(\Omega_m-1)+6x_\sigma^2-6x_\phi^2+4\Omega_r\big), \tag{13e}$$

$$\frac{d\lambda_\sigma}{dN}=-\sqrt{6}x_\sigma f(\lambda_\sigma), \tag{13f}$$

$$\frac{d\lambda_\phi}{dN}=-\sqrt{6}x_\phi g(\lambda_\phi), \tag{13g}$$

where $N=\ln a$ is the number of e-foldings, $f(\lambda_\sigma)=\lambda_\sigma^2(\Gamma_\sigma-1)$, $g(\lambda_\phi)=\lambda_\phi^2(\Gamma_\phi-1)$ and:

$$\Gamma_\sigma=\frac{V_\sigma(\sigma)V_\sigma''(\sigma)}{(V_\sigma'(\sigma))^2}, \qquad \Gamma_\phi=\frac{V_\phi(\phi)V_\phi''(\phi)}{(V_\phi'(\phi))^2}. \tag{14}$$

In order to get from the autonomous equations (13) a closed system of ordinary differential equations we have assumed that the functions Γ_σ and Γ_ϕ can be written as a function of the variables $\lambda_\sigma \in \mathbb{R}$ and $\lambda_\phi \in \mathbb{R}$ respectively [34].

The phase space for the autonomous dynamical system (13) can be defined as follows:

$$\begin{aligned}\Psi=\big\{&(x_\sigma, x_\phi, y_\sigma, \Omega_r, \Omega_m)\in\mathbb{R}^5:\ y_\sigma\geqslant 0,\ 0\leqslant\Omega_{\rm DE}\leqslant 1,\\ &x_\sigma^2-x_\phi^2+y_\sigma^2+\Omega_r+\Omega_m\leqslant 1,\\ &0\leqslant\Omega_r\leqslant 1,\ 0\leqslant\Omega_m\leqslant 1\big\}\times\big\{(\lambda_\sigma,\lambda_\phi)\in\mathbb{R}^2\big\},\end{aligned} \tag{15}$$

where

$$\Omega_{\rm DE}\equiv\Omega_\sigma+\Omega_\phi=1-\Omega_r-\Omega_m, \tag{16a}$$

follows from definitions (10).

Now, with the aim of explaining the physical significance of the critical points of the autonomous system (13) we need to obtain the relevant cosmological parameters in terms of the dimensionless phase space variables (12a). Following this, the cosmological parameters (8), (9) and (10) can be expressed as

$$w_{\rm DE}=\frac{2x_\sigma^2-2x_\phi^2+\Omega_m+\Omega_r-1}{1-\Omega_m-\Omega_r} \tag{17a}$$

$$w_{\rm tot}=-1+\Omega_m+2x_\sigma^2-2x_\phi^2+\frac{4\Omega_r}{3} \tag{17b}$$

$$\Omega_\sigma=x_\sigma^2+y_\sigma^2, \tag{17c}$$

$$\Omega_\phi=1-\Omega_\sigma-\Omega_r-\Omega_m, \tag{17d}$$

while the deceleration parameter becomes

$$q=-\left[1+\frac{\dot H}{H^2}\right]=-1+\frac{3\Omega_m}{2}+3x_\sigma^2-3x_\phi^2+2\Omega_r. \tag{18}$$

Observe that: $w_{\rm tot}=\frac{2q-1}{3}$.

4. Critical points and stability

The critical points of the system (13) are summarized in Table 1. The eigenvalues of the corresponding Jacobian matrices are shown in Table 2, while the basic observables evaluated at the critical points are displayed in Table 3. In all cases, λ_σ^* and λ_ϕ^* are the values which make the functions $f(\lambda_\sigma)=\lambda_\sigma^2(\Gamma_\sigma-1)$ and $g(\lambda_\phi)=\lambda_\phi^2(\Gamma_\phi-1)$ vanish respectively.

As we see from Table 1, the points $P_1^\pm$ do not exist in the strict sense (x_ϕ is purely imaginary at the fixed points). Point P_5 (resp. P_6) is associated with a combination of a phantom (resp. quintessence) potential whose first ϕ-derivative (resp. σ-derivative) vanishes at some/several point/points, i.e., $\lambda_\phi=0$ (resp. $\lambda_\sigma=0$), and an arbitrary self interaction potential for the quintessence (resp. phantom) component, i.e., for arbitrary value of λ_σ (resp. λ_ϕ). For the point P_7, both $\lambda_\phi=0$ and $\lambda_\phi=0$.

Table 2
Eigenvalues of the linear perturbation matrix associated to each of the critical points displayed in Table 1. The upper asterisk is used to denote values of λ_σ and λ_ϕ such that $\lambda_\sigma \in f^{-1}(0)$ and $\lambda_\phi \in g^{-1}(0)$, i.e., $f(\lambda_\sigma^*)=0$ and $g(\lambda_\phi^*)=0$, respectively. Here we use the definitions $\frac{1}{\lambda^2}=\frac{1}{(\lambda_\sigma^*)^2}-\frac{1}{(\lambda_\phi^*)^2}$, $\Delta_1^\pm=-\frac{3}{2}(1\pm\sqrt{1+\frac{4}{3}g(0)})$, $\Delta_2^\pm=-\frac{3}{2}(1\pm\sqrt{1-\frac{4}{3}f(0)})$, $\Delta_3^\pm=-\frac{3}{2}(1\pm\sqrt{1-\frac{4}{3}f(0)y_\sigma^2})$, $\Delta_4^\pm=-\frac{3}{2}(1\pm\sqrt{1+\frac{4}{3}g(0)(1-y_\sigma^2)})$, $\chi^\pm(z)=-\frac{1}{2}(1\pm\sqrt{\frac{64}{z^2}-15})$, and $\eta^\pm(z)=-\frac{3}{4}(1\pm\sqrt{\frac{24}{z^2}-7})$ where z is a dummy variable.

Label	m_1	m_2	m_3	m_4	m_5	m_6	m_7
$P_1^\pm$	3	0	0	$\mp i\sqrt{6}g'(\lambda_\phi^*)$	$6\mp i\sqrt{6}\lambda_\phi^*$	2	3
$P_2^\pm$	6	0	0	$\mp\sqrt{6}f'(\lambda_\sigma^*)$	$3\mp\sqrt{\frac{3}{2}}\lambda_\sigma^*$	2	3
$P_3^\pm$	0	$-\sqrt{6}g'(\lambda_\phi^*)x_\phi$	$\mp\sqrt{6}f'(\lambda_\sigma^*)\sqrt{1+x_\phi^2}$	$3\mp\sqrt{\frac{3}{2}}\sqrt{1+x_\phi^2}\lambda_\sigma^*$	$6-\sqrt{6}x_\phi\lambda_\phi^*$	2	3
P_4	0	$-f'(\lambda_\sigma^*)\lambda_\sigma^*$	$(\lambda\sigma^*)^2$	$\frac{1}{2}((\lambda_\sigma^*)^2-6)$	$\frac{1}{2}((\lambda_\sigma^*)^2-6)$	$(\lambda_\sigma^*)^2-4$	$(\lambda_\sigma^*)^2-3$
P_5	-3	0	0	Δ_1^+	Δ_1^-	-4	-3
P_6	-3	0	0	Δ_2^+	Δ_2^-	-4	-3
P_7	0	Δ_3^+	Δ_3^-	Δ_4^+	Δ_4^-	-4	-3
P_8	0	$g'(\lambda_\phi^*)\lambda_\phi^*$	$-\frac{1}{2}(\lambda_\phi^*)^2$	$-\frac{1}{2}((\lambda_\phi^*)^2+6)$	$-\frac{1}{2}((\lambda_\phi^*)^2+6)$	$-(\lambda_\phi^*)^2-4$	$-(\lambda_\phi^*)^2-3$
P_9	4	2	-1	-1	0	0	1
P_{10}	4	-1	0	1	$\chi^+(\lambda_\sigma^*)$	$\chi^-(\lambda_\sigma^*)$	$-\frac{4f'(\lambda_\sigma^*)}{\lambda_\sigma^*}$
P_{11}	$-\frac{1}{2}+\frac{i\sqrt{15}}{2}$	$-\frac{1}{2}-\frac{i\sqrt{15}}{2}$	1	$\chi^+(\lambda)$	$\chi^-(\lambda)$	$-\frac{4f'(\lambda_\sigma^*)}{\lambda_\sigma^*}$	$-\frac{4g'(\lambda_\phi^*)}{\lambda_\phi^*}$
P_{12}	0	0	$\frac{3}{2}$	3	$-\frac{3}{2}$	$-\frac{3}{2}$	-1
P_{13}	0	$-\frac{3}{2}$	3	-1	$\eta^+(\lambda_\sigma^*)$	$\eta^-(\lambda_\sigma^*)$	$-\frac{3f'(\lambda_\sigma^*)}{\lambda_\sigma^*}$
P_{14}	$-\frac{3}{4}(1+i\sqrt{7})$	$-\frac{3}{4}(1-i\sqrt{7})$	-1	$\eta^+(\lambda)$	$\eta^-(\lambda)$	$-\frac{3f'(\lambda_\sigma^*)}{\lambda_\sigma^*}$	$-\frac{3g'(\lambda_\phi^*)}{\lambda_\phi^*}$

Table 3
Basic observables evaluated at the critical points of the autonomous system (13). The upper asterisk is used to denote values of λ_σ and λ_ϕ such that $\lambda_\sigma \in f^{-1}(0)$ and $\lambda_\phi \in g^{-1}(0)$, i.e., $f(\lambda_\sigma^*)=0$ and $g(\lambda_\phi^*)=0$, respectively.

Label	Ω_r	Ω_m	$\Omega_{\rm DE}$	q	$w_{\rm DE}$	$w_{\rm tot}$
$P_1^\pm$	0	0	1	2	1	1
$P_2^\pm$	0	0	1	2	1	1
$P_3^\pm$	0	0	1	2	1	1
P_4	0	0	1	$-1+\frac{(\lambda_\sigma^*)^2}{2}$	$-1+\frac{(\lambda_\sigma^*)^2}{3}$	$-1+\frac{(\lambda_\sigma^*)^2}{3}$
P_5	0	0	1	-1	-1	-1
P_6	0	0	1	-1	-1	-1
P_7	0	0	1	-1	-1	-1
P_8	0	0	1	$-1-\frac{(\lambda_\phi^*)^2}{2}$	$-1-\frac{(\lambda_\phi^*)^2}{3}$	$-1-\frac{(\lambda_\phi^*)^2}{3}$
P_9	1	0	0	1	Indeterminate	$\frac{1}{3}$
P_{10}	$1-\frac{4}{(\lambda_\sigma^*)^2}$	0	$\frac{4}{(\lambda_\sigma^*)^2}$	1	$\frac{1}{3}$	$\frac{1}{3}$
P_{11}	$1-\frac{4}{\lambda^2}$	0	$\frac{4}{\lambda^2}$	1	$\frac{1}{3}$	$\frac{1}{3}$
P_{12}	0	1	0	$\frac{1}{2}$	Indeterminate	0
P_{13}	0	$1-\frac{3}{(\lambda_\sigma^*)^2}$	$\frac{3}{(\lambda_\sigma^*)^2}$	$\frac{1}{2}$	0	0
P_{14}	0	$1-\frac{3}{\lambda^2}$	$\frac{3}{\lambda^2}$	$\frac{1}{2}$	0	0

It is worth noticing that the existence conditions for the rest of the points displayed in Table 1 depends of the concrete form of the potential. Besides, from the table of the eigenvalues (Table 2) follows that all the points, with the exception of P_{11} and P_{14}, belong to nonhyperbolic sets of critical point with a least one null eigenvalue.

For these nonhyperbolic sets, we are not able to extract information about their stability by using the standard tools of the linear dynamical analysis, unless they were normally hyperbolic sets. We recall that an invariant set of non-isolated singular points is normally-hyperbolic if the equilibrium set has only one zero eigenvalue at each point, all other eigenvalues have non-zero real parts, and the eigenvector associated to the zero eigenvalue is tangent to the set. Thus its stability is determined by the sign of the remaining non-null eigenvalues. Nonhyperbolic fixed points, with both non-empty stable and unstable subspaces, will have saddle behavior. In case that the standard linear dynamical systems analysis fails to be applied, then we need to rely our analysis on numer-

ical inspection of the phase portrait for specific potentials or using more sophisticated techniques like the Center Manifold Theory (for technical discussions see Refs. [22,23,46–48]).

4.1. Stability of the critical points

Although all these critical points are shown in Table 1 here we have summarized their basic properties:

- $P_1^{\pm}$, $P_2^{\pm}$ and $P_3^{\pm}$ correspond to a solution dominated by the kinetic energy of the scalar fields (stiff fluid solution: $q=2$ and $w_{\rm tot}=1$). The exact cosmological behavior differs for each point. $P_1^{\pm}$ corresponds to a phantom kinetic energy-dominated solutions ($\Omega_\sigma=0$ and $\Omega_\phi=1$). However, these points have a purely imaginary values of x_ϕ, thus, they do not exist in the strict sense. They have a three-dimensional center subspace and a four-dimensional unstable manifold (m_1, m_6, $m_7>0$, $\Re(m_5)>0$). Thus they cannot be late-time attractors. $P_2^{\pm}$ are dominated by the quintessence kinetic term ($\Omega_\sigma=1$ and $\Omega_\phi=0$), they are non-hyperbolic due to the existence of two null eigenvalues, so, as commented before we are not able to extract information about their stability by using the standard tools of the linear dynamical analysis. However, since for these points the unstable manifold is at least 3D, then, typically, they are unstable (a local source or a saddle depending on the parameter choices). $P_3^{\pm}$ represent solutions dominated by the kinetic energies of both the quintessence and phantom fields ($\Omega_\sigma=1+x_\phi^2$ and $\Omega_{\rm DE}=1$), i.e., the cosmic evolution is dominated by the kinetic term of the quintom field. These points depend of the form of the potentials and under certain conditions they have a six-dimensional unstable subspace which could correspond to the past attractor, otherwise it is a saddle point. In fact P_3^{+} has a 6D unstable manifold for either:
  (i) $x_\phi<0$, $\lambda_\sigma^*<\sqrt{\frac{6}{1+x_\phi^2}}$, $\lambda_\phi^*>\frac{\sqrt{6}}{x_\phi}$, $f'(\lambda_\sigma^*)<0$, $g'(\lambda_\phi^*)>0$, or
  (ii) $x_\phi>0$, $\lambda_\sigma^*<\sqrt{\frac{6}{1+x_\phi^2}}$, $\lambda_\phi^*<\sqrt{\frac{6}{1+x_\phi^2}}$, $f'(\lambda_\sigma^*)<0$, $g'(\lambda_\phi^*)<0$;
  whereas P_3^{-} has a 6D unstable manifold for either:
  (i) $x_\phi<0$, $\lambda_\sigma^*>-\sqrt{\frac{6}{1+x_\phi^2}}$, $\lambda_\phi^*>\frac{\sqrt{6}}{x_\phi}$, $f'(\lambda_\sigma^*)>0$, $g'(\lambda_\phi^*)>0$, or
  (ii) $x_\phi>0$, $\lambda_\sigma^*>-\sqrt{\frac{6}{1+x_\phi^2}}$, $\lambda_\phi^*<\frac{\sqrt{6}}{x_\phi}$, $f'(\lambda_\sigma^*)>0$, $g'(\lambda_\phi^*)<0$.
  $P_3^{\pm}$ contains, as a particular case, the points $P_2^{\pm}$ for the choice $x_\phi=0$, $g(\lambda_\phi)=0$.
  None of the these critical points are relevant for the late-time dynamics, thus the corresponding center manifold calculation and its stability analysis is not presented.
- P_4 is a scaling solution between the kinetic and the potential energy of the quintessence component of dark energy. This solution in sensitive to the explicit form of the potential. This is always a saddle equilibrium point in the phase space since for example $m_2=(\lambda_\sigma^*)^2$ and $m_4=\frac{1}{2}((\lambda_\sigma^*)^2-6)$ are of opposite sign in the existence region of this point. It represents an accelerated solution for a potential $V_\sigma(\sigma)$ whose function $f(\lambda_\sigma)$ vanish for $\lambda_\sigma=\lambda_\sigma^*$ in the interval $-\sqrt{2}<\lambda_\sigma^*<\sqrt{2}$, leading to a $-1\leqslant w_{\rm tot}<-1/3$. When $\lambda_\sigma^*=0$ the critical point P_4 becomes in P_6. In the regions $-\sqrt{6}\leqslant\lambda_\sigma^*\leqslant-\sqrt{2}$ or $\sqrt{2}\leqslant\lambda_\sigma^*\leqslant\sqrt{6}$, the critical point P_4 represents a non-accelerated phase. A very interesting issue of this critical point appears when the quintessence field is able to mimic the behavior of radiation ($w_r=1/3$) or dark matter ($w_m=0$) at background level. This happens when, for an specific form of the quintessence potential, $\lambda_\sigma^*=\pm2$ leading to $w_{\rm tot}=1/3$ or $\lambda_\sigma^*=\pm\sqrt{3}$ driving to $w_{\rm tot}=0$ respectively.[5]
- P_5, P_6 and P_7 represent solutions dominated by the potential energies of the potentials (all of them represent de Sitter solutions: $q=-1$ and $w_{\rm tot}=-1$). Once again the exact cosmological nature of them differs from one point to the other: P_5 is dominated by the potential energy of the phantom component ($\Omega_\sigma=0$ and $\Omega_\phi=1$). Because of the existence of two null eigenvalues is not possible to conclude about its dynamics from the linear analysis. However, it has a five-dimensional stable manifold for $g(0)<0$ (in the interval $g(0)<-\frac{3}{4}$ it has to complex conjugated eigenvalues with negative real parts). In these cases it is worthy to analyze its stability using the center manifold theory. P_6 is a critical point dominated by the quintessence potential energy term ($\Omega_\sigma=1$ and $\Omega_\phi=0$), despite its nonhyperbolicity, it has five-dimensional stable manifold for $f(0)>0$ (in the case $f(0)>\frac{3}{4}$, it has to complex conjugated eigenvalues with negative real parts), thus, it is worthy to analyze its stability using the center manifold theory. P_7 denotes a segment (curve) of non-isolated fixed points, representing a scaling regimen between the quintessence and phantom potential ($\Omega_\sigma=y_\sigma^2$ and $\Omega_\phi=1-y_\sigma^2$). It is normally-hyperbolic, since the eigenvector associated to the zero eigenvalue, $(0,0,1,0,0)^T$, is tangent to the curve. Thus its stability is determined by the sign of the remaining non-null eigenvalues. Hence, it is stable for $f(0)>0$, $g(0)<0$ or a saddle otherwise.
- P_8 is a line of fixed points parametrized by $\lambda_\sigma\in\mathbb{R}$ and it is normally-hyperbolic, due to the eigenvector associated to the zero eigenvalue, $(0,0,0,1,0)^T$, is tangent to the curve. Like P_7, its stability is determined by the sign of the remaining non-null eigenvalues. From Table 2 follows that P_8 admits a six-dimensional stable subspace provided $g'(\lambda_\phi^*)\lambda_\phi^*<0$, thus, the invariant curve is stable for these parameter conditions. It represents accelerated solutions dominated by the phantom potential ($\Omega_\sigma=0$ and $\Omega_\phi=1$) providing a crossing through the phantom divide. For every value of λ_ϕ^* this point provides the super-accelerated expansion typical of the quintom paradigm ($w_{\rm tot}=-1-\frac{(\lambda_\phi^*)^2}{3}$) the only exception occurs when $\lambda_\phi^*=0$ recovering the behavior of the de Sitter solution P_5 ($w_{\rm tot}=-1$). This line of critical points corresponds to the stable point P in [21] and B in [18] (phantom-dominated solution). Summarizing, the line P_8 is the late-time stable attractor provided $g'(\lambda_\phi^*)\lambda_\phi^*<0$, otherwise, it is a saddle point.
- P_9 corresponds to a radiation-dominated solution ($\Omega_r=1$) which is a saddle point since the stable manifold is 2D and the unstable one is 3D.
- P_{10} represents a scaling radiation-quintessence solution which is a saddle because at least two eigenvalues have different signs, say $m_1=4$ and $m_2=-1$.
- P_{11} represents a scaling radiation–DE (quintom) solution which is a saddle because at least two eigenvalues have reals parts of different signs, say $\Re(m_1)=-\frac{1}{2}$ and $m_2=1$. Thus, P_9, P_{10} and P_{11} correspond to transient stages for the cosmic evolution which corresponds to an effective radiation source ($w_{\rm tot}=\frac{1}{3}$), so they cannot represent the late-time universe.
- P_{12} corresponds to a dark-matter-dominated universe ($\Omega_m=1$) which is a saddle point since the stable manifold is 3D and the unstable one is 2D.
- P_{13} represents a scaling dark matter–quintessence solution. It is a saddle because at least two eigenvalues have different signs, say $m_2=-\frac{3}{2}$ and $m_3=3$. Summarizing, P_{12} and P_{13},

[5] See next subsection for a detailed discussion about this critical point.

which corresponds to an effective dust source ($w_{\rm tot}=0$), are transient stages for the cosmic evolution, and thus they are not good candidates for the late-time universe.

- P_{14} corresponds to scaling dark matter–DE (quintom) solution which can be either stable or saddle depending on choice of the parameters.

Actually, P_{14} is stable for either:

(i) $\lambda_\sigma^*\leqslant-\sqrt{3}$, $\lambda_\phi^*<0$, $f'(\lambda_\sigma^*)<0$, $g'(\lambda_\phi^*)<0$, or
(ii) $\lambda_\sigma^*\leqslant-\sqrt{3}$, $\lambda_\phi^*>0$, $f'(\lambda_\sigma^*)<0$, $g'(\lambda_\phi^*)>0$, or
(iii) $-\sqrt{3}<\lambda_\sigma^*<0$, $-\sqrt{\frac{3(\lambda_\sigma^*)^2}{3-(\lambda_\sigma^*)^2}}<\lambda_\phi^*<0$, $f'(\lambda_\sigma^*)<0$, $g'(\lambda_\phi^*)<0$, or
(iv) $-\sqrt{3}<\lambda_\sigma^*<0$, $0<\lambda_\phi^*<\sqrt{\frac{3(\lambda_\sigma^*)^2}{3-(\lambda_\sigma^*)^2}}$, $f'(\lambda_\sigma^*)<0$, $g'(\lambda_\phi^*)>0$, or
(v) $0<\lambda_\sigma^*<\sqrt{3}$, $-\sqrt{\frac{3(\lambda_\sigma^*)^2}{3-(\lambda_\sigma^*)^2}}<\lambda_\phi^*<0$, $f'(\lambda_\sigma^*)>0$, $g'(\lambda_\phi^*)<0$, or
(vi) $0<\lambda_\sigma^*<\sqrt{3}$, $0<\lambda_\phi^*<\sqrt{\frac{3(\lambda_\sigma^*)^2}{3-(\lambda_\sigma^*)^2}}$, $f'(\lambda_\sigma^*)>0$, $g'(\lambda_\phi^*)>0$, or
(vii) $\lambda_\sigma^*\geqslant\sqrt{3}$, $\lambda_\phi^*<0$, $f'(\lambda_\sigma^*)>0$, $g'(\lambda_\phi^*)<0$, or
(viii) $\lambda_\sigma^*\geqslant\sqrt{3}$, $\lambda_\phi^*>0$, $f'(\lambda_\sigma^*)>0$, $g'(\lambda_\phi^*)>0$.

It is a saddle otherwise.

When P_{14} is stable, it provides a good candidate for solving or alleviating the coincidence problem (why $\Omega_m\sim\Omega_{\rm DE}$ nowadays?). However, since in this case it corresponds to an effective dust source ($w_{\rm tot}=0$), then, it is unlikely that this point represents accurately the late-time universe. But if we restrict the parameter space in order to avoid all the above conditions (i)–(viii), but preserving the existence condition $0\leqslant\frac{3}{\lambda^2}\leqslant1$, where $\frac{1}{\lambda^2}=\frac{1}{(\lambda_\sigma^*)^2}-\frac{1}{(\lambda_\phi^*)^2}$, we obtain that P_{14} will be a saddle point, thus representing a transient stage of the cosmic evolution.[6]

4.2. Cosmological consequences

As was shown in the previous subsection the autonomous system (13) only admits fifteen classes of critical points (some of them are actually curves of fixed points).[7] The curves $P_2^{\pm}$ correspond to decelerated solutions, with $q=2$, where the Friedmann constraint (2a) is dominated by the kinetic energy of the quintessence field with an stiff-like equation of state, $w_{\rm tot}=1$. These solutions are only relevant at early times [44].

In order that our model can be in line with the current observational data, it must have to follow a *complete cosmological dynamics* [49], namely: it should describe an early radiation-dominated era (RDE), later enter into an epoch of mater domination (MDE), and finally reproduce the present speed up of the Universe. At each of these stages some special forms of matter seems to dominate the evolution, and the required dominance should be translated in different critical points, around which cosmological solutions remain a lapse of time, before ultimately approaching an stable late-time configuration. In the dynamical systems language a complete cosmological dynamics can be understood as an heteroclinic orbit connecting a past attractor, also called source, with a late-time attractor, also called sink, that passes through some saddle points, such that a RDE precedes a MDE. Recall that critical points are often the extreme points of the orbits and therefore describe the asymptotic behavior. However, there are solutions that interpolate between critical points, and then, they provide information of the intermediate stages of the evolution. These kind of solutions can be divided into heteroclinic orbit and homoclinic orbit (that looks like closed loop). The heteroclinic orbit connects two different critical points and the homoclinic orbit is an orbit connecting a critical point to itself. We are interested in heteroclinic orbits that should correspond to an specific cosmological history where a RDE precedes a MDE and thus, following a complete cosmological dynamics. We submit the reader to Refs. [22,23,50,51], for recent discussions on the role of heteroclinic orbits in cosmology.

The condition for a purely RDE ($\Omega_r=1$) is satisfied by P_9, this critical point always exists with a saddle behavior. As Table 3 shown, P_9 represents a decelerating expansion solution with $q=1$. For certain potentials, another possible critical points for a RDE, with saddle behavior, would be the decelerating expansion solutions ($q=1$) P_{10} and P_{11}.[8] In both cases, the dark energy component is able to mimic a radiation like fluid with $w_{\rm DE}=1/3$ (see Table 3). In order to recover a period dominated by radiation, we need to check the bounds imposed by the Big Bang Nucleosynthesis over the allowed amount of dark energy [52–57]. This bound comes from the primordial abundances of the light elements at the BBN ($T\approx1$ MeV) time. The current upper bound on the dark energy density at redshift of BBN ($z=10^9$) was obtained in [56]: $\Omega_{\rm DE}^{max}\leqslant0.064$ at 3σ, then this implies[9]:

$$P_{10}:\quad \Omega_{\rm DE}=\frac{4}{(\lambda_\sigma^*)^2}<0.064\quad\Rightarrow\quad\left(\lambda_\sigma^*\right)^2>62.5 \tag{19}$$

$$P_{11}:\quad \Omega_{\rm DE}=\frac{1}{\lambda^2}<0.064. \tag{20}$$

Although the value of the total (effective) equation of state parameter for P_{10} and P_{11} implies that, at the background level, they are able to describe a radiation-like expansion ($w_{\rm tot}=1/3$), it is mandatory to fulfill the previous conditions (19)–(20) in order to be a realistic RDE, otherwise there is a relic abundance problem.[10]

As we mention before, the Universe requires the existence of a long enough MDE in order to explain the formation of the cosmic structure. In our system, this period is recovered by a pure dark matter critical point P_{12} ($\Omega_m=1$), which corresponds to a decelerated expansion solution with $q=1/2$. As Table 1 shows, the existence of this point is always guaranteed in the phase space (15). As in the case of RDE, is possible to obtain two additional critical points with saddle behavior that may be associated with a MDE: P_{13} and P_{14}. Both critical points represent scaling solutions between the dark matter and the quintom field, where this latter component mimics a pressureless fluid ($w_{\rm DE}=0$, see Table 3). In order to recover a MDE ($\Omega_m\approx1$ and $\Omega_{\rm DE}\approx0$), the following conditions must be met[11]:

$$P_{13}:\quad\left(\lambda_\sigma^*\right)^2\gg3, \tag{21}$$

$$P_{14}:\quad\frac{1}{\lambda^2}\ll3. \tag{22}$$

As in the case of critical points P_{10} and P_{11} in the RDE, the existence of P_{13} and P_{14} depends of the explicit form of the potentials. Both pairs of critical points are *related*, namely:

[6] The trivial way to avoid this unwanted late-time behavior is choosing $\frac{3}{\lambda^2}>1$ which immediately gives that P_{14} does not exist.

[7] $P_1^{\pm}$ is ruled out because of they lead to imaginary values of dimensionless variable x_ϕ.

[8] As Table 1 shown, the existence of both critical points is sensitive to the explicit form of the potential.

[9] Recall that we used the definition $\frac{1}{\lambda^2}=\frac{1}{(\lambda_\sigma^*)^2}-\frac{1}{(\lambda_\phi^*)^2}$.

[10] See [44] for a similar analysis in exponential potential quintessence model.

[11] The value of $w_{\rm tot}=0$ for P_{13} and P_{14} implies that, at background level, both critical points are able to match a MDE, even if (21)–(22) are not satisfied.

- if P_{10} exists for a given potential, then P_{13} will exist as well.
- if P_{11} exists for a given potential, then P_{14} will exist as well.

In both cases the opposite statement is not necessarily true. Despite being *related*, the saddle nature of their behavior does not guarantee that initial conditions lead orbits to connect both groups of critical points, e.g.: $P_{10} \longrightarrow P_{13}$.

An interesting result comes from the stability of critical point P_4. This point exists if $-\sqrt{6} \leqslant \lambda_\sigma^* \leqslant \sqrt{6}$ and always behaves as a saddle fixed point. As Table 1 shown, its existence condition is independent of whether the radiation and cold dark matter are considered since $\Omega_r = \Omega_m = 0$. In the case of this point, as we mentioned before, if the quintessence potential fulfill the condition:

$$\lambda_\sigma^* = \pm 2, \tag{23}$$

then the effective equation of state of this dark energy component would mimic a radiation fluid ($w_{\rm DE} = w_{\rm tot} = 1/3$) or if:

$$\lambda_\sigma^* = \pm\sqrt{3}, \tag{24}$$

then the dark energy component would mimic pressureless fluid ($w_{\rm tot} = 0$), in other words: it will dynamically behave exactly as radiation (23) or cold dark matter (24) at background level. However, this statement is no enough to guarantee a realistic RDE. Since a null value of Ω_r ($\Omega_{\rm DE} = 1$) implies a relic abundance problem at BBN period [44], P_4 is ruled out as true period of radiation domination. The possibility of this dynamical characteristic impose a fine tuning over the shape of quintessence potentials and a priori there is no guarantee that all possible quintessence potentials may satisfy the above conditions (23)–(24).

Another important feature of the model is the presence of three accelerated solutions, described by critical points P_5, P_6 and P_7. All of them are de Sitter solutions ($w_{\rm tot} = -1$) dominated by the potentials of the scalar fields. P_5 and P_6 have a saddle behavior but P_7 can be stable for $f(0) > 0$, $g(0) < 0$ or a saddle otherwise. A favorable scenario would be one in which the initial conditions lead to a *complete cosmological dynamics*, e.g.: $P_2 \longrightarrow P_9 \longrightarrow P_{12}$, and then the orbits tend to one of the de Sitter solutions with saddle behavior P_5, P_6, and finally approaching either the late-time de Sitter point P_7 or the late time phantom attractor P_8. In terms of the cosmological evolution of the Universe, the above favorable scenario implies that the Universe started at early times from an stage dominated by the kinetic energy of the quintessence field, then evolve into an RDE from which, a MDE emerge to finally enter in the final phase of accelerated expansion. This accelerated phase can be the de Sitter solutions or a phantom-dominated solution ($w_{\rm tot} < -1$).[12] This final stage of evolutions towards critical point P_8 is consistent with the observational results from [12,13] which suggest a mild preference for a dark energy equation-of-state parameter in the phantom region ($w_{\rm tot} < -1$).

Finally, in order to examine the stability of the nonhyperbolic points that cannot consistently be studied via the present linear analysis, we present a concrete example. We provide a numerical elaboration of the phase space orbits of the corresponding quintom model.

4.3. $V(\sigma, \phi) = V_0 \sinh^2(\alpha\sigma) + V_1 \cosh^2(\beta\phi)$

This potential is derived, in a Friedmann–Robertson–Walker cosmological model, from canonical quantum cosmology under determined conditions in the evolution of our universe, using the Bohmian formalism [29,33].

For this potential:

$$f(\lambda_\sigma) = -\frac{\lambda_\sigma^2}{2} + 2\alpha^2, \qquad \lambda_\sigma^* = \pm 2\alpha, \qquad f'\big(\lambda_\sigma^*\big) = -\lambda_\sigma^* \tag{25}$$

and

$$g(\lambda_\phi) = -\frac{\lambda_\phi^2}{2} + 2\beta^2, \qquad \lambda_\phi^* = \pm 2\beta, \qquad g'\big(\lambda_\phi^*\big) = -\lambda_\phi^*. \tag{26}$$

Substituting the functions (25) and (26) in (13f) and (13g), respectively, we deduce the equations

$$\frac{d(\lambda_\sigma \pm 2\alpha)}{dN} = \frac{\sqrt{6}}{2} x_\sigma (\lambda_\sigma \mp 2\alpha)(\lambda_\sigma \pm 2\alpha), \tag{27}$$

$$\frac{d(\lambda_\phi \pm 2\beta)}{dN} = \frac{\sqrt{6}}{2} x_\phi (\lambda_\phi \mp 2\beta)(\lambda_\phi \pm 2\beta). \tag{28}$$

Using elementary dynamical systems theory follows from (27) and (28) that the subsets of the phase space given by $\lambda_\sigma \leqslant \pm 2\alpha$; $\lambda_\sigma = \pm 2\alpha$; $\lambda_\sigma \geqslant \pm 2\alpha$; $\lambda_\phi \leqslant \pm 2\beta$; $\lambda_\phi = \pm 2\beta$; and $\lambda_\phi \geqslant \pm 2\beta$ and their combinations (non-empty intersections and/or unions) are invariant sets for the flow of the dynamical system. This means, for example, that orbits initially in the strep $-2\beta < \lambda_\phi < 2\beta$, remain in this set for every time. These results allows to consider the dynamics restricted to several of these invariant sets since they act as independent dynamical objects, with the additional simplification of the dynamics.

From Table 2 and Eq. (26) we see that the condition to ensure that point P_8 has a four-dimensional stable subspace is always satisfied due to the opposite signs between λ_ϕ^* and $g'(\lambda_\phi^*)$.

To finish this section let's us discuss some numerical elaborations.

In Fig. 1 are presented the projections of some orbits of the phase space of the system (13) for the parameter choice $\alpha = \frac{\sqrt{5}}{2}$, $\beta = \frac{1}{2}$ at (a) the invariant set $\Omega_\sigma = 0, \Omega_r = 0, \Omega_m = 0$; (b) the subspace (Ω_r, Ω_r). For this choice of parameters the points P_{11} and P_{14} do not exist since at these points $\Omega_r < 0$. The remaining points in Table 1 always exist.

Fig. 1(a) captures the typical behavior in the plane (x_ϕ, λ_ϕ); i.e., we have two attractors: P_8 evaluated at the value $\lambda_\phi^* = +1$, labeled in the figure by P_{8a}, and P_{8b} which corresponds to the value $\lambda_\phi^* = -1$ irrespectively the initial values of Ω_σ, Ω_r, Ω_m. The phase space is divided in two portions where the attractor solution is either P_{8a} or P_{8b}. For the simulation in Fig. 1(b) we kept fixed the values $x_\sigma(0) = 0$, $y_\sigma(0) = 0$, $x_\phi(0) = 0$, $\lambda_\sigma(0) = 0$, $\lambda_\phi(0) = 0$ in all the initial conditions. In the figure it is shown that the matter-dominated epoch is a transient one preceded by a radiation-dominated epoch. Additionally these energy components become negligible late times.

In Fig. 2 are presented the projections of some orbits of the phase space of the system (13) for the parameter choice $\alpha = \frac{\sqrt{5}}{2}$, $\beta = \frac{1}{2}$ in the subspaces (a) $(x_\sigma, y_\sigma, x_\phi)$; (b) (x_σ, y_σ) and (c) (x_σ, x_ϕ). It is easy to see from the figures that the quintessence component tends to zero at late times dominating the phantom component. For the numerics we kept fixed the initial conditions $\Omega_r(0) = 10^{-5}$, $\Omega_m(0) = 0.3$, $\lambda_\phi(0) = -1$, $\lambda_\sigma(0) = \sqrt{5}$. It is worth noticing that $\lambda_\phi = -1, \lambda_\sigma = \sqrt{5}$ defines an invariant set. The attractor solution is always the phantom solution P_{8b}, i.e., the solution P_8 for the choice $\lambda_\phi^* = -1$. Choosing the initial value $\lambda_\phi(0) = +1$ the universe results at late times in the phantom solution P_{8a}.

[12] In fact, these models admit the possibility of having two stable solutions: a de Sitter solution (P_7) and a phantom solution (P_8), each one within their basin of attraction as was shown in previous subsection.

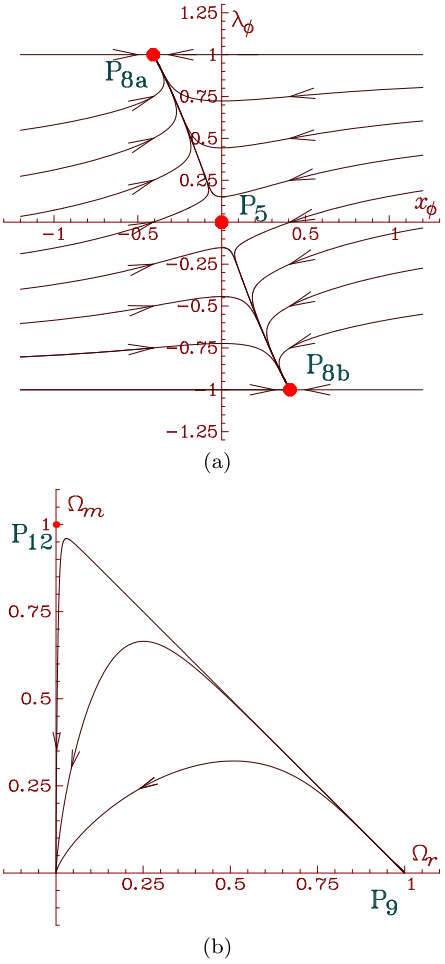

Fig. 1. Projections of some orbits of the phase space of the system (13) for the parameter choice $\alpha = \frac{\sqrt{5}}{2}$, $\beta = \frac{1}{2}$ at: (a) the invariant set $\Omega_\sigma = 0$, $\Omega_r = 0$, $\Omega_m = 0$ and (b) the subspace (Ω_r, Ω_m). In the figure (a) we have two attractors: P_{8a} which corresponds to the value $\lambda_\phi^* = +1$ and P_{8b} which corresponds to the value $\lambda_\phi^* = -1$ irrespectively the initial values of Ω_σ, Ω_r, Ω_m. The phase space is divided in two portions where the attractor solution is either P_{8a} or P_{8b}. For (b) we kept fixed the values $x_\sigma(0) = 0$, $y_\sigma(0) = 0$, $x_\phi(0) = 0$, $\lambda_\sigma(0) = 0$, $\lambda_\phi(0) = 0$ in all the initial conditions. In this figure, it is showed that the matter-dominated epoch is a transient one preceded by a radiation-dominated epoch. Additionally these energy components become negligible at late time, since the orbits tend to the origin as time goes forward.

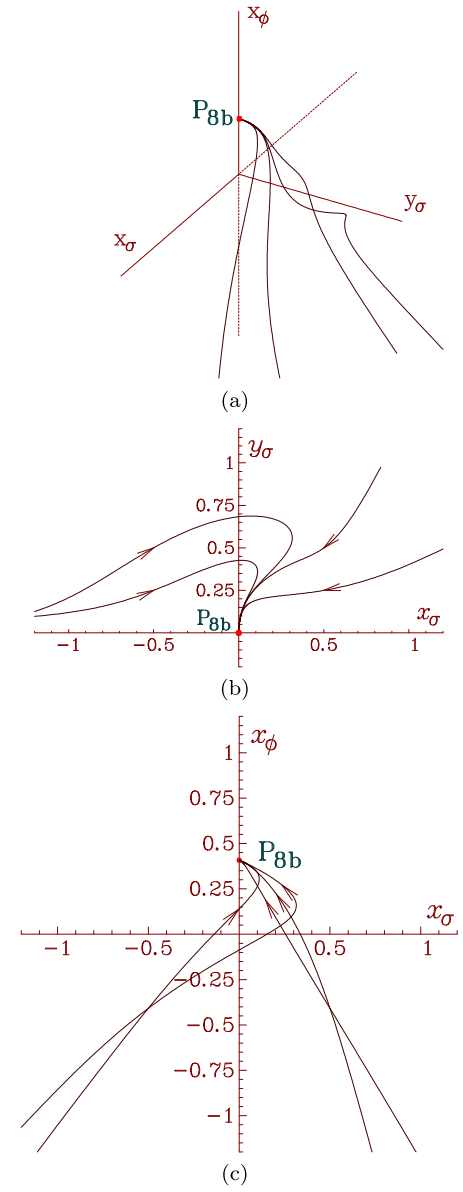

Fig. 2. Projections of some orbits of the phase space of the system (13) for the parameter choice $\alpha = \frac{\sqrt{5}}{2}$, $\beta = \frac{1}{2}$ in the subspaces (a) $(x_\sigma, y_\sigma, x_\phi)$; (b) (x_σ, y_σ) and (c) (x_σ, x_ϕ). For the numerics we kept fixed the values $\Omega_r(0) = 10^{-5}$, $\Omega_m(0) = 0.3$, $\lambda_\phi(0) = -1$, $\lambda_\sigma(0) = \sqrt{5}$ in all the initial conditions. It is worth to mention that $\lambda_\phi = -1$, $\lambda_\sigma = \sqrt{5}$ defines an invariant set. The attractor solution is always the phantom solution P_{8b}, i.e., the solution P_8 for the choice $\lambda_\phi^* = -1$.

5. Conclusions

In the present paper we studied a quintom dark energy model, that consists on an hybrid model with the simultaneously contribution of a canonical quintessence field and a phantom field. Additionally, we included dark matter and radiation that are represented by perfect fluids. An important assumption was that we only consider arbitrary decoupled potentials, which constrains the type of quintom dark energy scenarios covered by our analysis.

First, we conducted a comprehensive dynamical system analysis of the model in order to investigate both its asymptotic and intermediate evolution. Additionally, we demanded that our model must follow a *complete cosmological dynamics*: namely, the existence of a viable radiation dominate era (RDE) and a matter-dominated era (MDE) preceding to a late-time acceleration stage; these three different eras have to be present in any model of physical interest. The imposition of this requirement allows to demonstrate that this model is able to describe the aforementioned periods. Specifically, is possible to have three classes of solutions for the RDE: the standard pure radiation solution and two additional solutions, in which the dark energy component is able to mimic a radiation-like fluid. In the latter it was necessary to use the bounds imposed by the Big Bang Nucleosynthesis (BBN) over the allowed amount of dark energy at the RDE in order to constrains the free parameters of the quintom potentials. Similarly, four classes of solutions were found for the MDE: the standard pure dark matter solution, two scaling solutions between the dark matter and quintom field, where the dark energy component mimics a pressureless fluid. And for some especial conditions on the parameter space, is possible to obtain a saddle-like class of solutions where the quintessence field behaves as a dark matter at background level, even if radiation and dark matter are not considered in the setup of the model.

We presented general conditions on the quintom potentials for the stability of the phantom-dominated solutions (late time attractors), generalizing the results shown in [18,21] for exponential potentials. Under these conditions the Universe evolves from a quintessence-dominated phase to a phantom dominated phase, crossing the $w_{\rm tot} = -1$ divide line as a transient stage [58]. This important result is in correspondence with the cosmological observations that mildly favors the phantom regime [12,13].

An important feature of this model is the existence of three de Sitter solutions. The dynamical behavior of two of these solutions cannot be anticipated using the linearization due to their nonhyperbolic nature. Thus, to examine them, we employed the Center Manifold Theory. After deriving the evolution equation on the center manifolds and making several numerical integrations we have concluded that, in both cases, the corresponding de Sitter solution is unstable (saddle-like). In addition, it was shown that the remaining de Sitter solution, which is actually normally-hyperbolic, is stable under certain conditions, which makes it a viable late time solution.

For purposes of illustration, we have applied our general results to the specific quintom potential obtained from a canonical quantum cosmology [33].

Acknowledgements

Y.L. was partially supported by PROMEP, DAIP, and by CONACYT, México, under grants 167335 and 179881 and by PUCV through Proyecto DI Postdoctorado 2013 and 2014. G.L. was partially supported by PUCV through Proyecto DI Postdoctorado 2013, by Comisión Nacional de Ciencias y Tecnología through Proyecto FONDECYT de Postdoctorado 2014 grant 3140244 and by DI-PUCV grant 123.730/2013. G.L. and Y.L. wish to thank to their colleagues at Instituto de Física, Pontificia Universidad de Católica de Valparaíso, for their warm hospitality during the completion of this work. Y.L. is also grateful to the Departamento de Física and the CA de Gravitación y Física Matemática for their kind hospitality and their joint support for a postdoctoral fellowship.

Appendix A. Center manifold dynamics for the solution dominated by the potential energy of the phantom component P_5

In this section we apply the Center Manifold Theorem [22,23,46–48] to study the stability of non-hyperbolic point P_5 corresponding to the solution dominated by the potential energy of the phantom component. Without loosing generality we set $\Omega_r = 0$, $\Omega_m = 0$ in the following discussion.

First, we restrict our attention to the domain $-\frac{3}{4} < g(0) < 0$ to dealing with real eigenvalues.

The first step is to translate the point P_5 ($x_\sigma = 0$, $x_\phi = 0$, $y_\sigma = 0$, $\lambda_\sigma = \mu$, $\lambda_\phi = 0$) to the origin, where μ denotes an arbitrary value for λ_σ.

The next step is to transform the system to its real Jordan form:

$$\frac{d\mathbf{u}}{dN} = Z\mathbf{u} + F(\mathbf{u},\mathbf{v}) \tag{A.1}$$

$$\frac{d\mathbf{v}}{dN} = P\mathbf{v} + G(\mathbf{u},\mathbf{v}) \tag{A.2}$$

where the square matrices Z, P have 2 zero eigenvalues and 3 eigenvalues with negative real part, respectively. In order to do that we introduce the new variables:

$$u_1 = y_\sigma,$$
$$u_2 = -\sqrt{\frac{2}{3}}x_\sigma f(\mu) - \mu + \lambda_\sigma,$$
$$v_1 = \sqrt{\frac{2}{3}}x_\sigma f(\mu),$$
$$v_2 = \frac{2\sqrt{6}g(0)x_\phi + (\sqrt{12g(0)+9}-3)\lambda_\phi}{2\sqrt{12g(0)+9}},$$
$$v_3 = \frac{(\sqrt{12g(0)+9}+3)\lambda_\phi - 2\sqrt{6}g(0)x_\phi}{2\sqrt{12g(0)+9}}. \tag{A.3}$$

Using the above transformation, the system (A.1)–(A.2) is explicitly given by:

$$u_1' = F_1(u_1,u_2,v_1,v_2,v_3) \tag{A.4}$$

$$u_2' = -\frac{3v_1(f(\mu+u_2+v_1)-f(\mu))}{f(\mu)} + H(u_1,u_2,v_1,v_2,v_3) \equiv F_2(u_1,u_2,v_1,v_2,v_3) \tag{A.5}$$

$$v_1' = -3v_1 + G_1(u_1,u_2,v_1,v_2,v_3) \tag{A.6}$$

$$v_2' = \frac{1}{2}\big(-\sqrt{12g(0)+9}-3\big)v_2 + G_2(u_1,u_2,v_1,v_2,v_3) \tag{A.7}$$

$$v_3' = \frac{1}{2}\big(\sqrt{12g(0)+9}-3\big)v_3 + G_3(u_1,u_2,v_1,v_2,v_3), \tag{A.8}$$

where $f' = \frac{df}{dN}$, $F_1, H, G_1, \ldots, G_3$ are homogeneous polynomials of degree greater than 2 in the coordinates (u_1,u_2,v_1,v_2,v_3).

Following the standard formalism of the Center Manifold Theory, the coordinates which correspond to the non-zero eigenvalues (v_1,v_2,v_3) can be approximated by the functions:

$$k_1(u_1,u_2) = a_1u_1^2 + a_2u_1^3 + a_3u_1u_2 + a_4u_1^2u_2 + a_5u_2^2 + a_6u_1u_2^2 + a_7u_2^3 + \cdots + O\big(u_1^n,u_2^n\big) \tag{A.9}$$

$$k_2(u_1,u_2) = b_1u_1^2 + b_2u_1^3 + b_3u_1u_2 + b_4u_1^2u_2 + b_5u_2^2 + b_6u_1u_2^2 + b_7u_2^3 + \cdots + O\big(u_1^n,u_2^n\big) \tag{A.10}$$

$$k_3(u_1,u_2) = c_1u_1^2 + c_2u_1^3 + c_3u_1u_2 + c_4u_1^2u_2 + c_5u_2^2 + c_6u_1u_2^2 + c_7u_2^3 + \cdots + O\big(u_1^n,u_2^n\big) \tag{A.11}$$

with this set of functions we can solve, to any n desired degree of accuracy, the quasilinear partial differential equation for the center manifold:

$$Dk(\mathbf{u})\big[Z\mathbf{u} + F\big(\mathbf{u},k(\mathbf{u})\big)\big] - Pk(\mathbf{u}) - G\big(\mathbf{u},k(\mathbf{u})\big) = 0. \tag{A.12}$$

In our case: $Z = \left(\begin{smallmatrix}0&0\\0&0\end{smallmatrix}\right)$ and

$$P = \begin{pmatrix} -3 & 0 & 0 \\ 0 & \frac{1}{2}(-\sqrt{12g(0)+9}-3) & 0 \\ 0 & 0 & \frac{1}{2}(\sqrt{12g(0)+9}-3) \end{pmatrix}$$

$$k(\mathbf{u}) = \begin{pmatrix} k_1(u_1,u_2) \\ k_2(u_1,u_2) \\ k_3(u_1,u_2) \end{pmatrix}$$

$$Dk(\mathbf{u}) = \begin{pmatrix} \frac{\partial k_1}{\partial u_1} & \frac{\partial k_1}{\partial u_2} \\ \frac{\partial k_2}{\partial u_1} & \frac{\partial k_2}{\partial u_2} \\ \frac{\partial k_3}{\partial u_1} & \frac{\partial k_3}{\partial u_2} \end{pmatrix}$$

$$G\big(\mathbf{u},k(\mathbf{u})\big) = \begin{pmatrix} G_1(u_1,u_2,k_1(u_1,u_2),k_2(u_1,u_2),k_3(u_1,u_2)) \\ G_2(u_1,u_2,k_1(u_1,u_2),k_2(u_1,u_2),k_3(u_1,u_2)) \\ G_3(u_1,u_2,k_1(u_1,u_2),k_2(u_1,u_2),k_3(u_1,u_2)) \end{pmatrix}.$$

In order to solve equation (A.12) we put together Z, P, $k(u_1,u_2)$, $Dk(u_1,u_2)$ and $G(u_1,u_2,k(u_1,u_2))$, then we equate equal powers of u_1 and u_2, and in that way we compute $k(u_1,u_2)$. Finally we obtain, in the neighborhood of P_5, the reduced system:

$$\mathbf{u}' = Z\mathbf{u} + F\big(\mathbf{u}, k(\mathbf{u})\big). \tag{A.13}$$

Applying the above procedure to the equations (A.4)–(A.8) we get:

$$\begin{aligned} v_1 &= \frac{1}{3}\mu f(\mu)u_1^2 + \frac{1}{3}f(\mu)u_1^2u_2 + O(4),\\ v_2 &= v_3 = O(4). \end{aligned} \tag{A.14}$$

Neglecting the fourth order terms, the evolution equations on the center manifold are

$$u_1' = -\frac{1}{2}\mu^2 u_1^3, \tag{A.15}$$

$$u_2' = -u_1^2(\mu+u_2)f(\mu) - \mu u_1^2 u_2 f'(\mu). \tag{A.16}$$

For $\mu f'(\mu) + f(\mu) \neq 0$, the orbit of (A.15)–(A.16) passing through (u_{10}, u_{20}) is given by

$$\frac{u_1}{u_{10}} = \frac{1}{\sqrt{1+\mu^2 u_{10}^2 N}}, \quad N \geqslant 0, \tag{A.17}$$

$$u_2 = \big(\eta(\mu)+u_{20}\big)\left(\frac{u_1}{u_{10}}\right)^{\frac{2(\mu f'(\mu)+f(\mu))}{\mu^2}} - \eta(\mu), \tag{A.18}$$

where $\eta(\mu) = \frac{\mu f(\mu)}{\mu f'(\mu)+f(\mu)}$. Then, for $f(\mu)+\mu f'(\mu) > 0$, the orbits approach the point with coordinates $(u_1 = 0, u_2 = -\eta(\mu))$ when $N \to +\infty$. If $f(\mu)+\mu f'(\mu) \leqslant 0$, then, as $N \to +\infty$, u_1 tends to zero and u_2 becomes unbounded. Generically, the origin is not approached as $N \to +\infty$, unless $\mu f(\mu) = 0$.

In the special case $\mu f'(\mu) + f(\mu) = 0$, the system (A.15)–(A.16) reduces to

$$u_1' = -\frac{1}{2}\mu^2 u_1^3, \tag{A.19}$$

$$u_2' = -\mu f(\mu) u_1^2. \tag{A.20}$$

The orbit of (A.19)–(A.20) passing through (u_{10}, u_{20}) is given by

$$\frac{u_1}{u_{10}} = \frac{1}{\sqrt{1+\mu^2 u_{10}^2 N}}, \quad N \geqslant 0, \tag{A.21}$$

$$u_2 = u_{20} + \ln\left[\frac{u_1}{u_{10}}\right]^{\frac{2f(\mu)}{\mu}}. \tag{A.22}$$

In this case, u_1 tends to zero and u_2 becomes unbounded. Summarizing, for $-\frac{3}{4} < g(0) < 0$, P_5 is unstable.

For $g(0) < -\frac{3}{4}$, there are two complex eigenvalues. In this case, in order to obtain the real Jordan form, we introduce the new variables

$$V_2 = \frac{v_2+v_3}{2}, \qquad V_3 = \frac{v_2-v_3}{2i}.$$

Using the above transformation, the system (A.1)–(A.2) is given explicitly by:

$$u_1' = \widetilde{F}_1(u_1,u_2,v_1,V_2,V_3), \tag{A.23}$$

$$u_2' = \widetilde{F}_2(u_1,u_2,v_1,V_2,V_3), \tag{A.24}$$

$$v_1' = -3v_1 + \widetilde{G}_1(u_1,u_2,v_1,V_2,V_3), \tag{A.25}$$

$$V_2' = -\frac{3}{2}V_2 - \frac{1}{2}\sqrt{-12g(0)-9}\,V_3 + \widetilde{G}_2(u_1,u_2,v_1,V_2,V_3), \tag{A.26}$$

$$V_3' = -\frac{1}{2}\sqrt{-12g(0)-9}\,V_2 - \frac{3}{2}V_3 + \widetilde{G}_3(u_1,u_2,v_1,V_2,V_3), \tag{A.27}$$

where $\widetilde{F}_1, \widetilde{G}_1, \ldots, \widetilde{G}_3$ are homogeneous real polynomials of degree greater than 2 in the coordinates (u_1,u_2,v_1,V_2,V_3). Using the same procedure as before, we obtain that the center manifold is given locally by the graph

$$\begin{aligned} v_1 &= \frac{1}{3}\mu f(\mu)u_1^2 + \frac{1}{3}f(\mu)u_1^2u_2 + O(4),\\ V_2 &= V_3 = O(4). \end{aligned} \tag{A.28}$$

Thus the dynamics on the center manifold is given by the system (A.15)–(A.16) analyzed before. Summarizing, for $g(0) < 0$, P_5 is unstable.

Appendix B. Center manifold dynamics for the solution dominated by the potential energy of the quintessence component P_6

Now, let us implement the center manifold calculation for the non-hyperbolic point P_6 (corresponding to the solution dominated by the potential energy of the quintessence component), and discuss about its stability, by means of the powerful Center Manifold Theory [22,23,46–48]. As before, we set $\Omega_r = 0$, $\Omega_m = 0$ for simplicity.

The first step is to translate the point P_6 ($x_\sigma = 0$, $x_\phi = 0$, $y_\sigma = 1$, $\lambda_\sigma = 0$, $\lambda_\phi = \nu$) to the origin, where ν denotes an arbitrary value for λ_ϕ.

The next step is to transform the system to its real Jordan form:

$$\dot{\mathbf{u}} = Z\mathbf{u} + F(\mathbf{u},\mathbf{v}), \tag{B.1}$$

$$\dot{\mathbf{v}} = P\mathbf{v} + G(\mathbf{u},\mathbf{v}), \tag{B.2}$$

where the square matrices Z, P have 2 zero eigenvalues and 3 eigenvalues with negative real part, respectively.

In order to do that we introduce the new variables:

$$\begin{aligned} u_1 &= -2\nu(y_\sigma - 1)g(\nu),\\ u_2 &= -\frac{1}{3}g(\nu)\big(\sqrt{6}x_\phi - 2\nu(y_\sigma-1)\big) - \nu + \lambda_\phi,\\ v_1 &= \frac{1}{3}g(\nu)\big(\sqrt{6}x_\phi - 2\nu(y_\sigma-1)\big),\\ v_2 &= \frac{2\sqrt{6}f(0)x_\sigma + (\sqrt{9-12f(0)}-3)\lambda_\sigma}{2\sqrt{9-12f(0)}},\\ v_3 &= \frac{-2\sqrt{6}f(0)x_\sigma + (\sqrt{9-12f(0)}+3)\lambda_\sigma}{2\sqrt{9-12f(0)}}. \end{aligned} \tag{B.3}$$

Using the above transformation, the system (B.1)–(B.2) is given explicitly by:

$$u_1' = F_1(u_1,u_2,v_1,v_2,v_3), \tag{B.4}$$

$$\begin{aligned} u_2' = &-\frac{3v_1(g(\nu+u_2+v_1)-g(\nu))}{g(\nu)} + \frac{u_1 g(\nu+u_2+v_1)}{g(\nu)}\\ &+ H(u_1,u_2,v_1,v_2,v_3) \equiv F_2(u_1,u_2,v_1,v_2,v_3), \end{aligned} \tag{B.5}$$

$$v_1' = -3v_1 + G_1(u_1,u_2,v_1,v_2,v_3), \tag{B.6}$$

$$v_2' = \frac{1}{2}\big(-\sqrt{9-12f(0)}-3\big)v_2 + G_2(u_1,u_2,v_1,v_2,v_3), \tag{B.7}$$

$$v_3' = \frac{1}{2}\big(\sqrt{9-12f(0)}-3\big)v_3 + G_3(u_1,u_2,v_1,v_2,v_3), \tag{B.8}$$

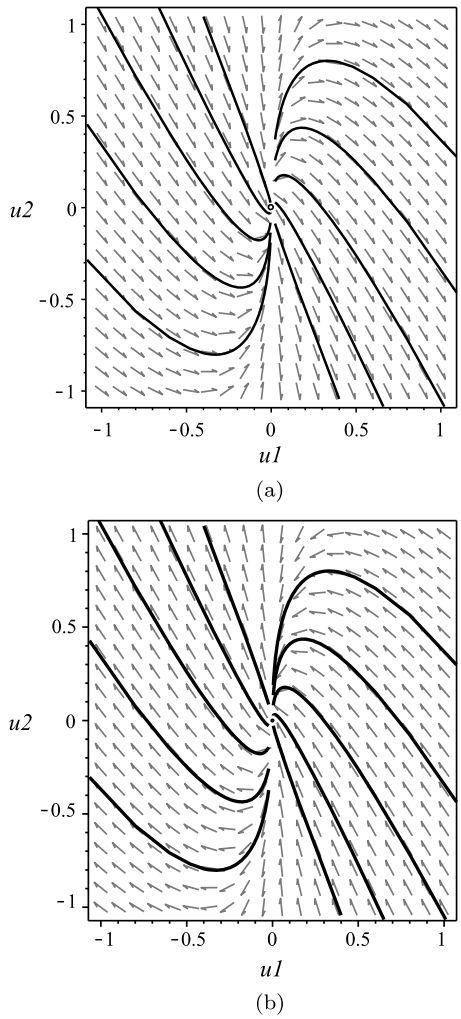

Fig. 3. Vector field in the plane (u_1, u_2) for the potential $V(\sigma,\phi) = V_0 \sinh^2(\alpha\sigma) + V_1 \cosh^2(\beta\phi)$. In (a), the free parameters have been chosen to be: $(\alpha,\ \beta,\ \nu)$: $(-\sqrt{3}/2,\ 0.35,\ 0.50)$. In this case $g(\nu) = 0.12 > 0$. The sign of u_1 is invariant. For $u_1 < 0$ the origin is approached as the time goes forward whereas for $u_1 > 0$ the orbits depart from the origin. In (b) the free parameters have been chosen to be: $(\alpha,\ \beta,\ \nu)$: $(-\sqrt{3}/2,\ 0.35,\ -0.50)$. The orbits are the same as in (a), with the arrows in reverse orientation. Thus, the accelerated de Sitter solution P_6 is a transient era in the evolution of the Universe.

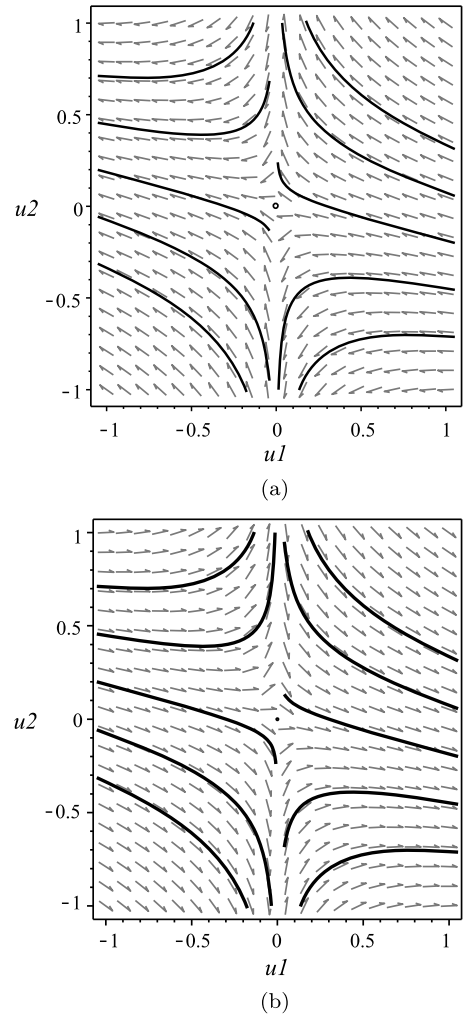

Fig. 4. Vector field in the plane (u_1, u_2) for the potential $V(\sigma,\phi) = V_0 \sinh^2(\alpha\sigma) + V_1 \cosh^2(\beta\phi)$. In (a) the free parameters have been chosen to be $(\alpha,\ \beta,\ \nu)$: $(-\sqrt{3}/2,\ 0.35,\ 1.30)$. In this case $g(\nu) = -0.60 < 0$. In (b) the free parameters have been chosen to be $(\alpha,\ \beta,\ \nu)$: $(-\sqrt{3}/2,\ 0.35,\ -1.30)$. The orbits are the same as in (a), with the arrows in reverse orientation. This suggest that the origin is a saddle, thus the accelerated de Sitter solution P_6 is a transient era in the evolution of the Universe.

where $f' = \frac{df}{dN}$, and $F_1, H, G_1, \ldots, G_3$ are homogeneous polynomials of degree greater than 2 in the coordinates $(u_1, u_2, v_1, v_2, v_3)$.

Following the standard formalism of the Center Manifold Theory, we obtain that the center manifold of P_6 is given by the graph

$$v_1 = \frac{\nu u_1^2}{18 g(\nu)} + \frac{u_1^2}{12\nu g(\nu)} + \frac{u_1^2}{9\nu} - \frac{u_1 u_2}{3\nu} + O(3);$$
$$v_2 = O(3), \qquad v_3 = O(3). \tag{B.9}$$

Neglecting the third order terms, the evolution equations on the center manifold are

$$u_1' = \frac{\nu u_1^2}{g(\nu)}, \tag{B.10}$$

$$u_2' = \frac{u_1 u_2}{\nu} - \frac{(2\nu^2+3)u_1^2}{12\nu g(\nu)}. \tag{B.11}$$

Let us assume $g(\nu) \neq 0, \nu \neq 0$. Hence, the orbit of (B.10)–(B.11) passing through (u_{10}, u_{20}) is given by

$$u_2 = \frac{((2\nu^2+3)u_{10} + 12\nu^2 u_{20} - 12u_{20} g(\nu))}{12(\nu^2 - g(\nu))}\left(\frac{u_1}{u_{10}}\right)^{\frac{g(\nu)}{\nu^2}} + \frac{(2\nu^2+3)u_1}{12(g(\nu) - \nu^2)}, \tag{B.12}$$

$$\frac{u_1}{u_{10}} = \frac{g(\nu)}{g(\nu) - \nu u_{10} N}, \quad N \geqslant 0. \tag{B.13}$$

In order to investigate the stability of the center manifold of P_6 we have resorted to several numerical integrations of the system (B.10)–(B.11). We find four typical situations that suggest that P_6 is unstable (saddle type).

In Fig. 3(a) is displayed the vector field in the plane (u_1, u_2) for the potential $V(\sigma,\phi) = V_0 \sinh^2(\alpha\sigma) + V_1 \cosh^2(\beta\phi)$. The free parameter has been chosen to be $(\alpha,\ \beta,\ \nu)$: $(-\sqrt{3}/2,\ 0.35,\ 0.50)$. In this case $g(\nu) = 0.12 > 0$. The sign of u_1 is invariant. For $u_1 < 0$ the origin is approached as the time goes forward whereas for $u_1 > 0$ the orbits depart from the origin. On the other hand, for the choice $(\alpha,\ \beta,\ \nu)$: $(-\sqrt{3}/2,\ 0.35,\ -0.50)$ we have also $g(\nu) = 0.12 > 0$, additionally, the orbits are the same as in the former case, but the time flow is oriented in reverse. Both numerical elaborations suggest that the accelerated de Sitter solution P_6 (the

origin of coordinates), is a transient era in the evolution of the Universe for $g(\nu) > 0$ irrespectively the sign of ν.

Furthermore, in Fig. 4(a) is presented the vector field in the plane (u_1, u_2) for the same potential as before, but for the choice of parameters (α, β, ν): $(-\sqrt{3}/2, 0.35, 1.30)$. In this case $g(\nu) = -0.60 < 0$. The sign of u_1 is invariant. As shown is this figure, all the orbits depart from the origin. For the choice (α, β, ν): $(-\sqrt{3}/2, 0.35, -1.30)$, we have also $g(\nu) = -0.60 > 0$. In this case all the orbits are the same, they departs for the origin but with the arrows in reverse orientation as displayed in Fig. 4(b). Thus, summarizing, this numerical elaboration suggest that the accelerated de Sitter solution P_6, is a transient era in the evolution of the Universe for $g(\nu) < 0$ irrespectively the sign of ν.

As in Appendix A, for analyzing the case of complex eigenvalues, we can introduce the new variables

$$V_2 = \frac{\nu_2 + \nu_3}{2}, \qquad V_3 = \frac{\nu_2 - \nu_3}{2i}$$

for deriving the real Jordan form of the Jacobian. The procedure is straightforward, so we won't enter into the details here.

References

[1] Adam G. Riess, Lucas Macri, Stefano Casertano, Hubert Lampeitl, Henry C. Ferguson, et al., A 3% solution: determination of the Hubble constant with the Hubble Space Telescope and Wide Field Camera 3, Astrophys. J. 730 (2011) 119.

[2] E. Komatsu, et al., Seven-year Wilkinson Microwave Anisotropy Probe (WMAP) observations: cosmological interpretation, Astrophys. J. Suppl. Ser. 192 (18) (2011).

[3] Beth A. Reid, Will J. Percival, Daniel J. Eisenstein, Licia Verde, David N. Spergel, et al., Cosmological constraints from the clustering of the Sloan digital sky survey DR7 luminous red galaxies, Mon. Not. R. Astron. Soc. 404 (2010) 60–85.

[4] Hong Li, Xin Zhang, Probing the dynamics of dark energy with divergence-free parametrizations: a global fit study, Phys. Lett. B 703 (2011) 119–123.

[5] Ujjaini Alam, Varun Sahni, A.A. Starobinsky, The case for dynamical dark energy revisited, J. Cosmol. Astropart. Phys. 0406 (2004) 008.

[6] Bo Feng, Xiu-Lian Wang, Xin-Min Zhang, Dark energy constraints from the cosmic age and supernova, Phys. Lett. B 607 (2005) 35–41.

[7] Huterer Dragan, Asantha Cooray, Uncorrelated estimates of dark energy evolution, Phys. Rev. D 71 (2005) 023506.

[8] S. Nesseris, Leandros Perivolaropoulos, Crossing the phantom divide: theoretical implications and observational status, J. Cosmol. Astropart. Phys. 0701 (2007) 018.

[9] Harvinder K. Jassal, J.S. Bagla, T. Padmanabhan, Understanding the origin of CMB constraints on dark energy, Mon. Not. R. Astron. Soc. 405 (2010) 2639–2650.

[10] Bohdan Novosyadlyj, Olga Sergijenko, Ruth Durrer, Volodymyr Pelykh, Do the cosmological observational data prefer phantom dark energy? Phys. Rev. D 86 (2012) 083008.

[11] B. Novosyadlyj, O. Sergijenko, R. Durrer, V. Pelykh, Quintessence versus phantom dark energy: the arbitrating power of current and future observations, 2012.

[12] G. Hinshaw, D. Larson, E. Komatsu, D.N. Spergel, C.L. Bennett, et al., Nine-year Wilkinson Microwave Anisotropy Probe (WMAP) observations: cosmological parameter results, 2012.

[13] P.A.R. Ade, et al., Planck 2013 results. XVI. Cosmological parameters, 2013.

[14] Alexander Vikman, Can dark energy evolve to the phantom? Phys. Rev. D 71 (2005) 023515.

[15] Wayne Hu, Crossing the phantom divide: dark energy internal degrees of freedom, Phys. Rev. D 71 (2005) 047301.

[16] Robert R. Caldwell, Michael Doran, Dark-energy evolution across the cosmological-constant boundary, Phys. Rev. D 72 (2005) 043527.

[17] Jun-Qing Xia, Yi-Fu Cai, Tao-Tao Qiu, Gong-Bo Zhao, Xinmin Zhang, Constraints on the sound speed of dynamical dark energy, Int. J. Mod. Phys. D 17 (2008) 1229–1243.

[18] Yi-Fu Cai, Emmanuel N. Saridakis, Mohammad R. Setare, Jun-Qing Xia, Quintom cosmology: theoretical implications and observations, Phys. Rep. 493 (2010) 1–60.

[19] Cedric Deffayet, Oriol Pujolas, Ignacy Sawicki, Alexander Vikman, Imperfect dark energy from kinetic gravity braiding, J. Cosmol. Astropart. Phys. 1010 (2010) 026.

[20] Xiao-Fei Zhang, Hong Li, Yun-Song Piao, Xin-Min Zhang, Two-field models of dark energy with equation of state across -1, Mod. Phys. Lett. A 21 (2006) 231–242.

[21] Zong-Kuan Guo, Yun-Song Piao, Xin-Min Zhang, Yuan-Zhong Zhang, Cosmological evolution of a quintom model of dark energy, Phys. Lett. B 608 (2005) 177–182.

[22] J. Wainwright, G.F.R. Ellis, Dynamical Systems in Cosmology, Cambridge University Press, 2005.

[23] A.A. Coley, Dynamical Systems and Cosmology, Astrophysics and Space Science Library, Springer, 2003.

[24] Ruth Lazkoz, Genly Leon, Quintom cosmologies admitting either tracking or phantom attractors, Phys. Lett. B 638 (2006) 303–309.

[25] Ruth Lazkoz, Genly Leon, Israel Quiros, Quintom cosmologies with arbitrary potentials, Phys. Lett. B 649 (2007) 103–110.

[26] M.R. Setare, E.N. Saridakis, Quintom cosmology with general potentials, Int. J. Mod. Phys. D 18 (2009) 549–557.

[27] M.R. Setare, E.N. Saridakis, Quintom model with $O(N)$ symmetry, J. Cosmol. Astropart. Phys. 0809 (2008) 026.

[28] M.R. Setare, E.N. Saridakis, Quintom dark energy models with nearly flat potentials, Phys. Rev. D 79 (2009) 043005.

[29] W. Guzman, M. Sabido, J. Socorro, L. Arturo Urena-Lopez, Scalar potentials out of canonical quantum cosmology, Int. J. Mod. Phys. D 16 (2007) 641–654.

[30] J. Socorro, Marco D'Oleire, Inflation from supersymmetric quantum cosmology, Phys. Rev. D 82 (2010) 044008.

[31] David Bohm, A suggested interpretation of the quantum theory in terms of hidden variables. 1, Phys. Rev. 85 (1952) 166–179.

[32] V. Moncrief, M.P. Ryan, Amplitude real phase exact solutions for quantum mixmaster universes, Phys. Rev. D 44 (1991) 2375–2379.

[33] J. Socorro, Priscila Romero, Luis O. Pimentel, M. Aguero, Quintom potentials from quantum cosmology using the FRW cosmological model, Int. J. Theor. Phys. 52 (2013) 2722–2734.

[34] Wei Fang, Ying Li, Kai Zhang, Hui-Qing Lu, Exact analysis of scaling and dominant attractors beyond the exponential potential, Class. Quantum Gravity 26 (2009) 155005.

[35] Yoelsy Leyva, Dania Gonzalez, Tame Gonzalez, Tonatiuh Matos, Israel Quiros, Dynamics of a self-interacting scalar field trapped in the braneworld for a wide variety of self-interaction potentials, Phys. Rev. D 80 (2009) 044026.

[36] Dagoberto Escobar, Carlos R. Fadragas, Genly Leon, Yoelsy Leyva, Phase space analysis of quintessence fields trapped in a Randall–Sundrum braneworld: anisotropic Bianchi I brane with a positive dark radiation term, Class. Quantum Gravity 29 (2012) 175006.

[37] Dagoberto Escobar, Carlos R. Fadragas, Genly Leon, Yoelsy Leyva, Phase space analysis of quintessence fields trapped in a Randall–Sundrum braneworld: a refined study, Class. Quantum Gravity 29 (2012) 175005.

[38] Dagoberto Escobar, Carlos R. Fadragas, Genly Leon, Yoelsy Leyva, Asymptotic behavior of a scalar field with an arbitrary potential trapped on a Randall–Sundrum's braneworld: the effect of a negative dark radiation term on a Bianchi I brane, Astrophys. Space Sci. 349 (2014) 575–602.

[39] Tonatiuh Matos, Jose-Ruben Luevano, Israel Quiros, L. Arturo Urena-Lopez, Jose Alberto Vazquez, Dynamics of scalar field dark matter with a cosh-like potential, Phys. Rev. D 80 (2009) 123521.

[40] Israel Quiros, Tame Gonzalez, Dania Gonzalez, Yunelsy Napoles, Study of tachyon dynamics for broad classes of potentials, Class. Quantum Gravity 27 (2010) 215021.

[41] Wei Fang, Hui-Qing Lu, Dynamics of tachyon and phantom field beyond the inverse square potentials, Eur. Phys. J. C 68 (2010) 567–572.

[42] H. Farajollahi, A. Salehi, F. Tayebi, A. Ravanpak, Stability analysis in tachyonic potential chameleon cosmology, J. Cosmol. Astropart. Phys. 1105 (2011) 017.

[43] Kui Xiao, Jian-Yang Zhu, Stability analysis of an autonomous system in loop quantum cosmology, Phys. Rev. D 83 (2011) 083501.

[44] Edmund J. Copeland, Andrew R. Liddle, David Wands, Exponential potentials and cosmological scaling solutions, Phys. Rev. D 57 (1998) 4686–4690.

[45] Xi-ming Chen, Yun-gui Gong, Emmanuel N. Saridakis, Phase-space analysis of interacting phantom cosmology, J. Cosmol. Astropart. Phys. 0904 (2009) 001.

[46] B. Aulbach, Continuous and Discrete Dynamics Near Manifolds of Equilibria, Lecture Notes in Mathematics, Springer-Verlag, 1984.

[47] L. Perko, Differential Equations and Dynamical Systems, Texts in Applied Mathematics, Springer, 2001.

[48] S. Wiggins, Introduction to Applied Nonlinear Dynamical Systems and Chaos, Texts in Applied Mathematics, Springer, 2003.

[49] Arturo Avelino, Yoelsy Leyva, L. Arturo Urena-Lopez, Interacting viscous dark fluids, Phys. Rev. D 88 (2013) 123004.

[50] J. Mark Heinzle, Claes Uggla, Niklas Rohr, The cosmological billiard attractor, Adv. Theor. Math. Phys. 13 (2009) 293–407.

[51] L. Arturo Urena-Lopez, Unified description of the dynamics of quintessential scalar fields, J. Cosmol. Astropart. Phys. 1203 (2012) 035.

[52] Pedro G. Ferreira, Michael Joyce, Cosmology with a primordial scaling field, Phys. Rev. D 58 (1998) 023503.

[53] Rachel Bean, Steen H. Hansen, Alessandro Melchiorri, Early universe constraints

on a primordial scaling field, Phys. Rev. D 64 (2001) 103508.
[54] Rachel Bean, Steen H. Hansen, Alessandro Melchiorri, Constraining the dark universe, Nucl. Phys. B, Proc. Suppl. 110 (2002) 167–172.
[55] James P. Kneller, Gary Steigman, BBN and CMB constraints on dark energy, Phys. Rev. D 67 (2003) 063501.
[56] Gary Steigman, BBN and the CBR probe the early universe, AIP Conf. Proc. 903 (2007) 40–47.
[57] Edward L. Wright, Constraints on dark energy from supernovae, gamma ray bursts, acoustic oscillations, nucleosynthesis and large scale structure and the Hubble constant, Astrophys. J. 664 (2007) 633–639.
[58] Zong-Kuan Guo, Yun-Song Piao, Xinmin Zhang, Yuan-Zhong Zhang, Two-field quintom models in the w–w' plane, Phys. Rev. D 74 (2006) 127304.